Piezo1 and Piezo2 Are Essential Components of Distinct Mechanically Activated Cation Channels

Bertrand Coste,[1] Jayanti Mathur,[2] Manuela Schmidt,[1] Taryn J. Earley,[1] Sanjeev Ranade,[1] Matt J. Petrus,[2] Adrienne E. Dubin,[1] Ardem Patapoutian[1,2]*

Mechanical stimuli drive many physiological processes, including touch and pain sensation, hearing, and blood pressure regulation. Mechanically activated (MA) cation channel activities have been recorded in many cells, but the responsible molecules have not been identified. We characterized a rapidly adapting MA current in a mouse neuroblastoma cell line. Expression profiling and RNA interference knockdown of candidate genes identified *Piezo1* (*Fam38A*) to be required for MA currents in these cells. Piezo1 and related Piezo2 (Fam38B) are vertebrate multipass transmembrane proteins with homologs in invertebrates, plants, and protozoa. Overexpression of mouse Piezo1 or Piezo2 induced two kinetically distinct MA currents. Piezos are expressed in several tissues, and knockdown of Piezo2 in dorsal root ganglia neurons specifically reduced rapidly adapting MA currents. We propose that Piezos are components of MA cation channels.

Mechanotransduction, the conversion of mechanical force into biological signals, has crucial roles in physiology. In mammals, embryonic development, touch, pain, proprioception, hearing, adjustment of vascular tone and blood flow, flow sensing in kidney, lung growth and injury, bone and muscle homeostasis, as well as metastasis are all regulated by means of mechanotransduction (*1*, *2*). In plants, mechanical force strongly affects morphogenesis, for example, in lateral root formation (*3*). Unicellular organisms such as ciliates sense touch and change direction in response to a tactile stimulus (*4*). Mechanotransduction in vertebrate inner-ear hair cells is extremely rapid, implicating an ion channel directly activated by force (*5*). Indeed, calcium-permeable mechanically activated (MA) cationic currents have been described in various mechanosensitive cells (*2*, *3*, *6*, *7*). However, only few MA channels have been identified to date (*1*, *2*), and definitive candidates in vertebrate mechanosensation has yet to emerge.

Neuro2A cells express MA currents. To identify proteins involved in mechanotransduction, we sought a cell line that expresses a MA current similar to those recorded from primary cells (*8*). We screened several mouse and rat cell lines (Neuro2A, C2C12, NIH/3T3, Min-6, 50B11, F11, and PC12), applying force to the cell surface via a piezo-electrically driven glass probe while patch-clamp recording in the whole-cell configuration with another pipette (*6*, *8*, *9*). The Neuro2A (N2A) mouse neuroblastoma cell line expressed the most consistent MA currents and showed relatively faster kinetics of adaptation (decreased activity in response to a sustained stimulus) as compared with that of other cell lines, such as C2C12s (Fig. 1, A and B, and fig. S1, A to D). Current-voltage relationships of N2A and C2C12 MA currents were linear between –80 and +80 mV with reversal potentials (E_{rev}) at +6.6 and +6.7 mV, respectively, and inward currents were suppressed with N-methyl-D-glucamine (NMDG)–chloride external solutions, suggesting cationic nonselective

[1]Department of Cell Biology, The Scripps Research Institute (TSRI), La Jolla, CA 92037, USA. [2]Genomics Institute of the Novartis Research Foundation (GNF), San Diego, CA 92121, USA.

*To whom correspondence should be addressed. E-mail: ardem@scripps.edu

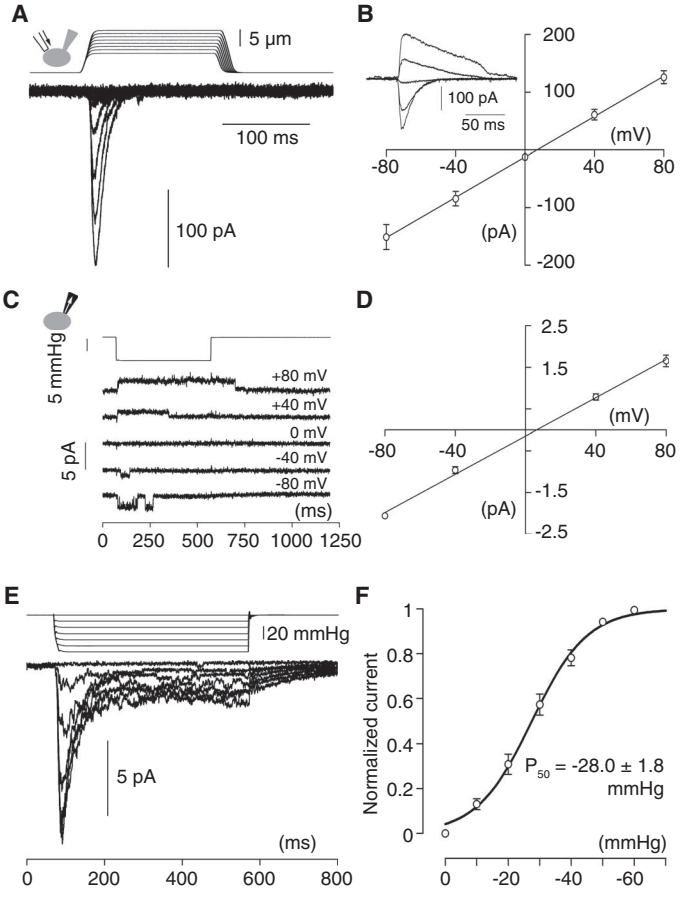

Fig. 1. MA currents in N2A cells. (**A**) Representative traces of MA inward currents expressed in N2A cells. Cells were subjected to a series of mechanical steps of 1-µm movements of a stimulation pipette (inset illustration, arrow) in the whole-cell patch configuration at a holding potential of –80 mV. (**B**) Average current-voltage relationships of MA currents in N2A cells (n = 11 cells). (Inset) Representative MA currents evoked at holding potentials ranging from –80 to +40 mV (applied 0.7 s before the mechanical step). (**C**) Single-channel currents (cell attached patch configuration) induced by means of negative pressure with a pipette (inset illustration, arrow) at holding potentials ranging from –80 mV to +80 mV in a N2A cell. (**D**) Average current-voltage relationships of stretch-activated single channels in N2A cells (n = 4 cells, mean ± SEM). Single-channel conductance was calculated from the slope of the linear regression line of each cell, giving γ = 22.9 ± 1.4 pS (mean ± SEM). Single-channel amplitude was determined as the amplitude difference in Gaussian fits of full-trace histograms. (**E**) Representative currents (averaged traces) induced by means of negative pipette pressure (0 to –60 mmHg, Δ 10 mmHg) in a N2A cell. (**F**) Normalized current-pressure relationship of stretch-activated currents at –80 mV fitted with a Boltzmann equation (n = 21 cells). P_{50} is the average value of P_{50} values from individual cells.

permeability (fig. S1E). We further characterized MA currents in N2A cells in response to suction of the membrane applied through the recording pipette in cell-attached mode (*10*). Negative pressure pulses evoked opening of endogenous channels (Fig. 1C), with a single-channel conductance of 22.9 ± 1.4 pS and E_{rev} of +6.2 mV (Fig. 1D). Increasing the magnitude of pressure pulses induced larger and reversible currents (Fig. 1E). The current-pressure relationship is characterized by maximal opening at –60 mmHg, with a pressure for half-maximal activation (P_{50}) of –28.0 ± 1.8 mmHg (Fig. 1F). These conductance and P_{50} values are similar to the properties of reported stretch-activated channels (*11*–*13*).

***Piezo1* (*Fam38A*) is required for MA currents of N2A cells.** To generate a list of candidate MA ion channels in N2A, we searched for

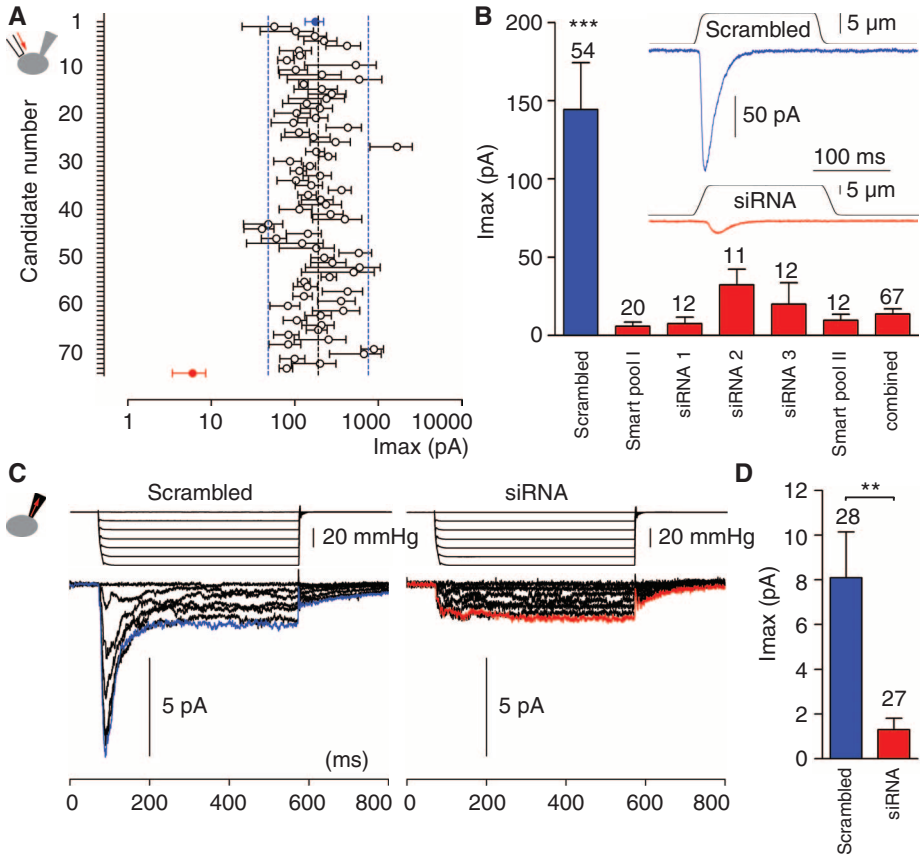

Fig. 2. Suppression of MA currents by means of Piezo1 (Fam38A) siRNA. (**A**) Average maximal amplitude of MA inward currents elicited at a holding potential of –80 mV in N2A cells transfected with scrambled siRNA (blue dot, n = 56 cells), Piezo1 (Fam38A) siRNA (red dot, n = 20 cells) or siRNA directed against other candidates tested (open symbols) (a list of candidates is available in table S1). For each candidate, the black circle and error bar represents the mean ± SEM, n = 4 to 27 cells each. The black line represents the average value of all cells tested (n = 807 cells), and the two blue dashed lines represent a fourfold decrease or increase of this value. (**B**) Average maximal amplitude of MA inward currents elicited at a holding potential of –80 mV in N2A cells transfected either with (blue) scrambled siRNA or (red) different Piezo1 (Fam38A) siRNAs. Smartpool I is composed of four siRNAs, including siRNA 1, 2, and 3. ***P < 0.001, Kruskal-Wallis test. (Inset) Representative traces of MA inward currents expressed in N2A cells transfected with (blue trace) scrambled siRNA or (red trace) Piezo1 (Fam38A) siRNA at a holding potential of –80 mV. (**C**) Representative currents (averaged traces) induced by means of negative pipette pressure (0 to –60 mmHg, Δ 10 mmHg, cell attached) in a N2A cell transfected with (left) scrambled siRNA or (right) Piezo1 siRNA. Traces of current elicited by –60 mmHg are highlighted in blue and red. (**D**) Average maximal amplitude of stretch-activated currents elicited at a holding potential of –80 mV in N2A cells transfected with (blue) scrambled siRNA or (red) Piezo1 siRNA. Bars represent the mean ± SEM, and the number of cells tested is shown above the bars. **P < 0.01, unpaired t test with Welch's correction.

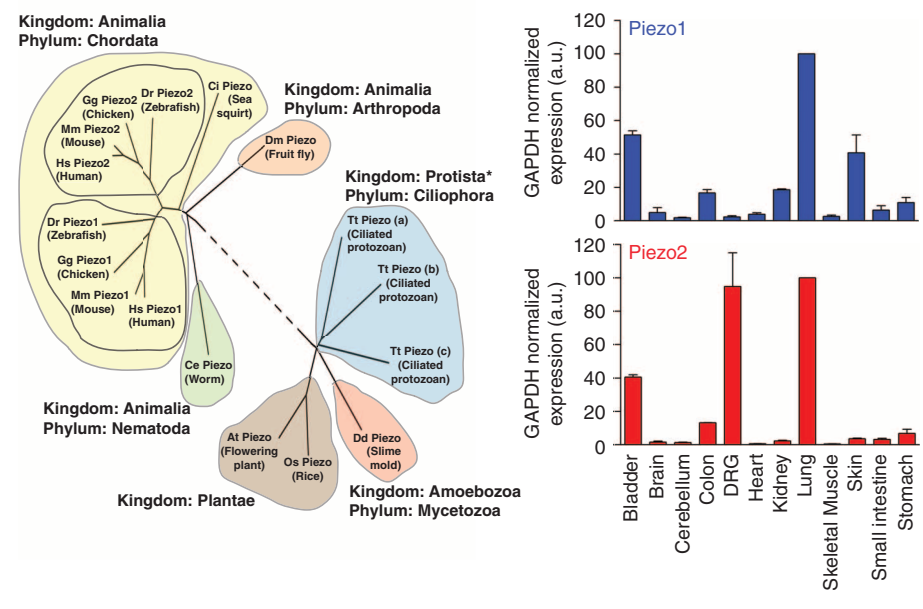

Fig. 3. Evolutionary conservation and expression profile of mouse Piezo1 and Piezo2. (**A**) Unrooted phylogenetic tree showing sequence relationship of different members of the Piezo family of proteins. The alignments were generated by using Megalign (DNASTAR, Madison, Wisconsin) and DrawTree programs. The dotted line represents an artificially extended line to accommodate fit. Hs, *Homo sapiens*; Mm, *Mouse musculus*; Gg, *Gallus gallus*, Dr, *Danio rerio*; Ci, *Ciona intestinalis*; Dm, *Drosophila melanogaster*; Ce, *Caenorhabditis elegans*; Dd, *Dictyostelium discoideum*; At, *Arabidopsis thaliana*; Os, *Oryza sativa*; and Tt, *Tetrahymena thermophila* [accession numbers are provided (*25*)]. Protista is referred to as a single kingdom but can be considered as a group of diverse phyla. (**B**) mRNA expression profiles of (top) *Piezo1* and (bottom) *Piezo2* determined by means of quantitative PCR from various adult mouse tissues. Glyceraldehyde-3-phosphate dehydrogenase (GAPDH) was used as the reference gene, and lung was used as the tissue calibrator by means of the $2^{-\Delta\Delta CT}$ method. Each bar is the mean + SEM of the average of two separate experiments.

transcripts that are enriched in N2A cells using Affymetrix microarrays (Affymetrix, Santa Clara, California). We selected proteins predicted to span the membrane at least two times (a characteristic shared by all ion channels). We prioritized this list by picking either known cation channels or proteins with unknown function. We tested each candidate (table S1) using small interfering RNA (siRNA) knockdown in N2A cells, measuring MA currents during piezo-driven pressure stimulation in the whole-cell mode. Knockdown of Fam38A (Family with sequence similarity 38) caused a pronounced decrease of MA currents (Fig. 2A). Attenuation of MA currents was observed with multiple siRNAs directed against this gene (Fig. 2B). All the siRNAs tested decreased the abundance of the target transcripts as assayed with quantitative polymerase chain reaction (PCR) (fig. S2A). Given that Fam38A encodes a protein required for the expression of ion channels activated by pressure, we named this gene Piezo1, from the Greek "πίεση" (píesi), meaning pressure. To test whether depletion of Piezo1 impairs general cell signaling or viability, we transfected N2A cells with TRPV1 cDNA (a capsaicin-activated cation channel) and either scrambled or Piezo1 siRNA and observed no differences in capsaicin responses (fig. S2, B and C). We tested whether Piezo1 was also required for N2A MA currents elicited through patch membrane stretch (Fig. 2C). MA currents were diminished in cells treated with siRNA against Piezo1 (Fig. 2D).

Very little is known about mammalian Piezo1 (KIAA0233, Fam38A, and Mib). Its expression is induced in senile plaque-associated astrocytes (*14*), and the protein has been suggested to be involved in integrin activation (*15*). Extracellular perfusion of cells with buffer lacking divalent ions and containing 5 mM EGTA for 30 to 60 min, which disrupts integrin function (*16*), did not suppress MA currents (fig. S2, D and E). Thus, it is unlikely that Piezo1 siRNA blocks MA currents through integrin modulation. However, it is possible that mechanical activation of Piezo1 could lead to integrin activation.

Piezos are large-transmembrane proteins conserved among various species. Many animal, plant, and other eukaryotic species contain a single Piezo (Fig. 3A). Vertebrates have two members, Piezo1 (Fam38A) and Piezo2 (Fam38B). However, the early chordate Ciona has a single member. Multiple Piezos are also present in the Ciliophora kingdom: *Tetrahymena thermophila* has three members; *Paramecium tetraurelia* has six. No clear homologs were identified in yeast or bacteria. The secondary structure and overall length of Piezo proteins are moderately conserved, and similarity to other proteins is minimal. As assayed with the Transmembrane Hidden Markov Model prediction program (TMHMM2) (CBS, Lyngby, Denmark), all have between 24 and 36 predicted transmembrane domains (with variability perhaps being due to inaccurate cDNA or transmembrane prediction). The predicted proteins contain 2100 to 4700 amino acids, and the transmembrane domains are located throughout the putative protein (fig. S3). Piezo1 expression was observed in bladder, colon, kidney, lung, and skin (Fig. 3B). This pattern agrees with Northern blot expression analysis in rat (*14*). Bladder, colon, and lung undergo mechanotransduction related to visceral pain (*17*), and primary cilia in the kidney sense urinary flux (*18*). The relatively low amount of mRNA in dorsal root ganglia (DRGs) suggests that Piezo1 may not account for MA currents observed there (*8*, *9*, *19*–*22*), but Piezo1 was observed in the skin, which is another putative site

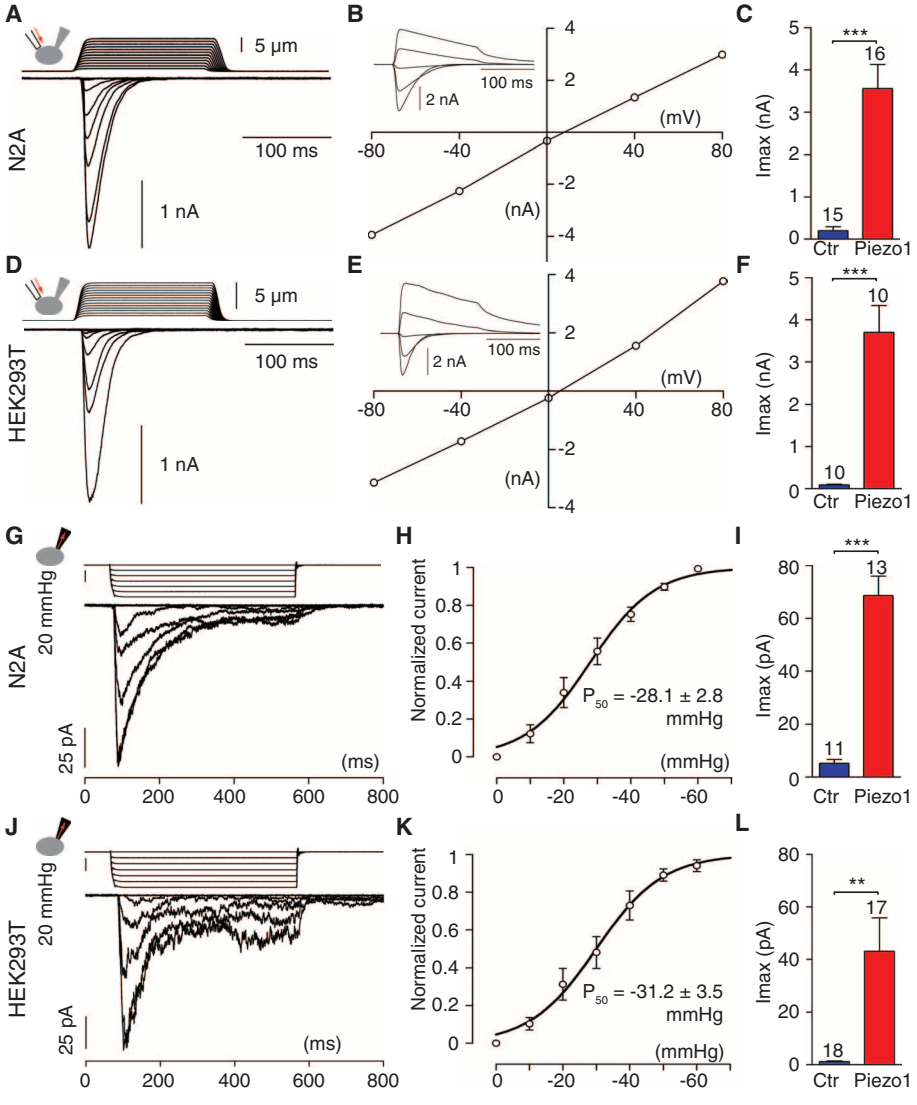

Fig. 4. Large MA currents from cells overexpressing Piezo1. (**A** to **F**) MA currents of Piezo1-expressing [(A) to (C)] N2A and [(D) to (F)] HEK293T cells recorded in the whole-cell configuration. [(A) and (D)] Representative traces of MA inward currents expressed in different cell types transfected with Piezo1. Cells were subjected to a series of mechanical steps in 1-μm (A) or 0.5-μm (D) increments by using glass probe stimulation and at a holding potential of −80 mV. [(B) and (E)] Representative current-voltage relationships of MA currents expressed in different cell types transfected with Piezo1. (Inset) MA currents evoked at holding potentials ranging from −80 to +40 mV. [(C) and (F)] Average maximal amplitude of MA inward currents elicited at a holding potential of −80 mV in (red) Piezo1-transfected or (blue) mock-transfected cells. Bars represent the mean ± SEM, and the number of cells tested is shown above the bars. ***$P < 0.001$, unpaired *t* test with Welch's correction. (**G** to **L**) Stretch-activated currents of mouse [(G) to (I)] Piezo1-expressing N2A and [(J) to (L)] HEK293T cells in cell-attached configuration. Representative averaged currents induced by means of negative pipette pressure (0 to −60 mmHg, Δ 10 mmHg) in (G) N2A and (J) HEK293T cells transfected with Piezo1. I_{max} normalized current-pressure relationship of stretch-activated currents elicited at −80 mV in Piezo1-transfected [(H) $n = 12$ cells] N2A and [(K) $n = 11$ cells] HEK293T cells and fitted with a Boltzmann equation. P_{50} is the average value of all P_{50} values determined for individual cells. Average maximal amplitude of stretch-activated currents elicited at a holding potential of −80 mV in (I) N2A and (L) HEK293T cells (blue) mock-transfected or (red) transfected with Piezo1. Bars represent the mean ± SEM, and the number of cells tested is shown above the bars. ***$P < 0.001$; **$P < 0.01$, unpaired *t* test with Welch's correction.

of somatosensation. Piezo2 expression was observed in bladder, colon, and lung as well, but less abundant in kidney or skin. Strong expression of Piezo2 was observed in DRG sensory neurons, suggesting a potential role in somatosensory mechanotransduction.

Piezo1 induces MA currents in various cell types. We cloned full-length *Piezo1* from N2A cells into the pIRES2–enhanced green fluorescent protein (EGFP) vector. We recorded MA currents from GFP-positive cells in the whole-cell mode 12 to 48 hours after transfection. *Piezo1* but not mock-transfected cells showed large MA currents in N2A, human embryonic kidney (HEK) 293 T (Fig. 4, A to F), and C2C12 cell lines (fig. S4, A to C). In all cells overexpressing Piezo1, the MA current-voltage relationships were similar to those for endogenous N2A MA currents (Fig. 4, B and E, and figs. 1B and S4B), with E_{rev} ~ +6 mV. The threshold of activation and the time constant for inactivation of MA currents elicited in Piezo1-overexpressing cells was similar in all three cell lines tested (table S2). We characterized the ionic selectivity of MA currents in cells overexpressing Piezo1. Substituting the nonpermeant cation NMDG in the extracellular bathing solution suppressed inward MA currents, demonstrating that this channel conducts cations (fig. S4, D and E). We further examined ionic selectivity by recording with CsCl-only internal solutions and various cations in the bath. Na^+, K^+, Ca^{2+} and Mg^{2+} all permeated, with a slight preference for Ca^{2+} (fig. S4, F to H). Moreover, 30 μM of ruthenium red and gadolinium, which are known blockers of many cationic MA currents (*9*, *23*), blocked 74.6 ± 2.5% (n = 6 cells) and 84.3 ± 3.8% (n = 5 cells) of Piezo1-induced MA current, respectively (fig. S4, I to K).

We used membrane stretch through the patch pipette in cell-attached mode to assay Piezo1-transfected cells (Fig. 4, G to L). Overexpression of Piezo1 in N2A and HEK293T cells gave rise to large currents elicited by –60 mmHg pressure pulses (Fig. 4, G and J). The current-pressure relationships in cells overexpressing Piezo1 and in endogenous N2A cells were similar, with P_{50} of –28.1 ± 2.8 and –31.2 ± 3.5 mmHg in N2A- and HEK293T-overexpressing cells, respectively (Figs. 1F and 4, H and K). No channel activity similar to N2A endogenous MA channels was detected in HEK293T cells transfected with vector alone.

MA currents in cells overexpressing Piezo2. We cloned full-length *Piezo2* from DRG neurons. N2A and HEK293T cells transfected with Piezo2 and gene-encoding GFP showed large MA currents (Fig. 5, A to F). The N2A cells were also cotransfected with Piezo1 siRNA to suppress endogenous MA currents. The MA current-voltage relationship in Piezo2-expressing cells was linear between –80 and +80 mV (Fig. 5, B and E), with a E_{rev} of +6.3 ± 0.4 mV (n = 3 cells) and +8.7 ± 1.5 mV (n = 7 cells) in N2A and HEK293T cells, respectively. Piezo2-dependent currents were suppressed by NMDG (fig. S5, A and B), suggesting nonselective cationic conductance. Piezo2-dependent currents were inhibited by gadolinium and ruthenium red [85.0 ± 3.7% (n = 5 cells) and 79.2 ± 4.2% (n = 5 cells), respectively] (fig. S5, C and D).

The inactivation kinetics of heterologously expressed Piezo2-induced MA currents were best

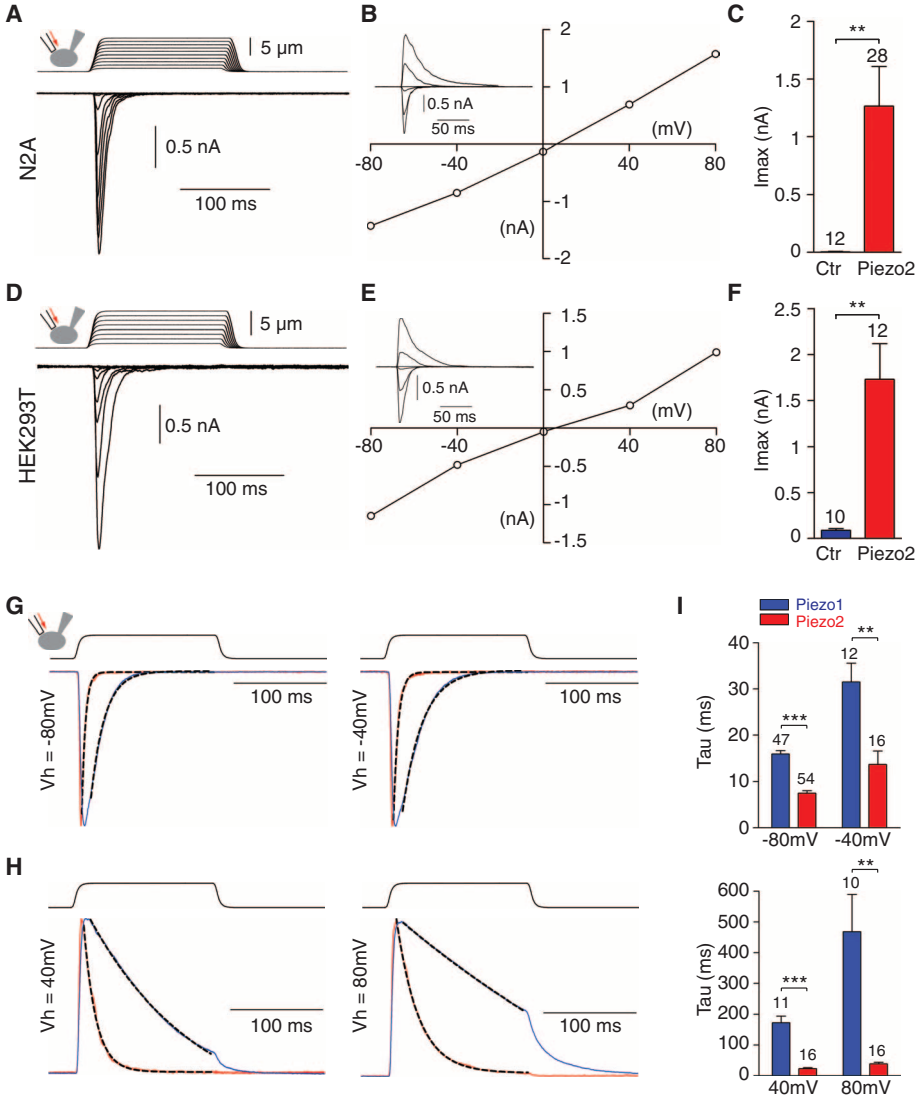

Fig. 5. Piezo2-dependent large MA currents kinetically distinct from Piezo1-induced currents. (**A** to **F**) MA currents of Piezo2-expressing [(A) to (C)] N2A and [(D) to (F)] HEK293T cells in whole-cell configuration. In N2A cells, Piezo2 or vector only were transfected with Piezo1 siRNA so as to suppress endogenous Piezo1-dependent MA currents. [(A) and (D)] Representative traces of MA inward currents expressed in different cell types transfected with Piezo2. Cells were subjected to a series of mechanical steps of 1-μm movements of a glass probe at a holding potential of –80 mV. [(B) and (E)] Representative current-voltage relationships of MA currents expressed in different cell types transfected with Piezo2. (Inset) MA currents evoked at holding potentials ranging from –80 to +40 mV. [(C) and (F)] Average maximal amplitude of MA inward currents elicited at a holding potential of –80 mV in (red) Piezo1-transfected or (blue) mock-transfected cells. (**G** and **H**) Representative traces of MA (G) inward or (H) outward currents expressed in cells transfected with (blue trace) Piezo1 or (red trace) Piezo2 at the specified holding potentials. Traces were normalized to the peak current, and dashed lines represent fits of inactivation with a mono-exponential equation. (**I**) Time-constant of inactivation of (blue) Piezo1 and (red) Piezo2 at negative (–80 and –40 mV, top) and positive (40 and 80 mV, bottom) holding potentials. Bars represent the mean ± SEM, and the numbers above bars are the number of cells. **P < 0.01; ***P < 0.001, unpaired t test with Welch's correction.

fitted with a mono-exponential equation. The calculated time constants for inactivation (τ_{inac}) are relatively fast in both N2A (6.8 ± 0.7 ms, n = 27 cells) and HEK293T (7.3 ± 0.7, n = 11 cells) cells when measured at –80 mV. Furthermore, the kinetics of inactivation of Piezo2-dependent MA currents were faster than Piezo1-dependent MA currents, both for inward (Fig. 5G) and outward (Fig. 5H) currents, and at all holding potentials tested (Fig. 5I). Therefore, Piezo1 and Piezo2 confer distinct channel properties.

Piezo1 is detected at the plasma membrane. The results above suggest that Piezo1 and Piezo2 are components of mechanotransduction complexes and therefore should be present at the plasma membrane. Previous reports have shown expression of Fam38A (Piezo1) in the endoplasmic reticulum (*14*, *15*). We generated a peptide antibody against mouse Piezo1. This antibody specifically recognized Piezo1-transfected HEK293T cells but not untransfected HEK293T cells (fig. S6A). In cells transfected with Piezo1 and TRPA1—an ion channel known to be expressed at the plasma membrane—we observed some overlap of Piezo1 staining with that of TRPA1 on the cell surface (*24*), although most Piezo1 and TRPA1 was present inside the cell (fig. S6B). Thus, Piezo1 protein can be localized at or near the plasma membrane. We could not detect expression of endogenous Piezo1 protein in N2A cells with this antibody.

Requirement of Piezo2 for rapidly adapting MA currents in DRG neurons. To characterize Piezo2 expression within the heterogeneous population of neurons and glial cells of the DRGs, we performed in situ hybridization on adult mouse DRG sections (Fig. 6A). We observed Piezo2 mRNA expression in 20% of DRG neurons (from 2391 total neurons) (*25*). Piezo2 was expressed in a subset of DRG neurons also expressing peripherin (60%) and neurofilament 200 (28%), which are markers present in mechanosensory neurons (*26*–*29*) (fig. S7). Some overlap with nociceptive marker TRPV1 (24%), further suggesting a potential role of Piezo2 in noxious mechanosensation. We used siRNA transfection to examine the role of Piezo2 in MA currents of DRG neurons. RNA interference (RNAi) on DRG neurons were validated on TRPA1, an ion channel expressed in DRG neurons and activated by mustard oil (MO) (*30*, *31*) (fig. S8, A and B). siRNAs against Piezo2 were validated in N2A cells overexpressing Piezo2 cDNA (fig. S8C). We recorded whole-cell MA currents from DRG neurons transfected with GFP and either scrambled or Piezo2 siRNA (n = 101 neurons for scrambled and n = 109 neurons for Piezo2 siRNA). We grouped the recorded MA currents according to their inactivation kinetics (Fig. 6B) (*8*, *9*, *19*, *20*, *22*). We defined four different classes of neurons on the basis of τ_{inac} distribution in scrambled siRNA transfected cells (Fig. S8D): $\tau_{inac} < 10$ ms, $10 < \tau_{inac} < 30$, $\tau_{inac} > 30$ ms, and nonresponsive neurons. The proportion of neurons expressing MA currents with $\tau_{inac} < 10$ ms was specifically and significantly reduced in neurons transfected with Piezo2 siRNA as compared with that of neurons transfected with scrambled siRNA (Fig. 6C). 28.7% of scrambled siRNA-transfected neurons had $\tau_{inac} < 10$ ms, compared with 7.3% in Piezo2 siRNA-transfected neurons (Fig. 6D). Neurons with MA currents with slower kinetics (τ_{inac} between 10 and 30 ms and $\tau_{inac} > 30$ ms) were present at normal proportions in cells transfected with Piezo2 siRNA. We observed a trend toward increased numbers of mechanically insensitive neurons in populations expressing Piezo2 siRNA, as predicted if loss of Piezo2 converts rapidly adapting neurons into nonresponders. We also analyzed these RNAi data according to the degree of current inactivation during the 150-ms test pulse and came to similar conclusions (fig. S8E).

Discussion. We found that Piezo1 is required for MA currents in Neuro2A cells and that Piezo2 is required for a subset of MA currents in DRG neurons. Moreover, overexpressing Piezo1 or Piezo2 in three different cell types gave rise to a 17- to 300-fold increase in MA currents. We conclude that Piezos are both necessary and sufficient for the expression of a MA current in various cell types.

Piezo1 and Piezo2 sequences do not resemble those of other known ion channels or other protein classes. The large number of predicted transmembrane domains of Piezo1 and Piezo2 is reminiscent of the structure of voltage-activated sodium channels with 24 transmembrane domains, composed of a fourfold repeat of six-transmembrane units (*32*). However, pore-containing or repetitive domains have not been observed in Piezo proteins. It may be that Piezo proteins are nonconducting subunits of ion channels required for

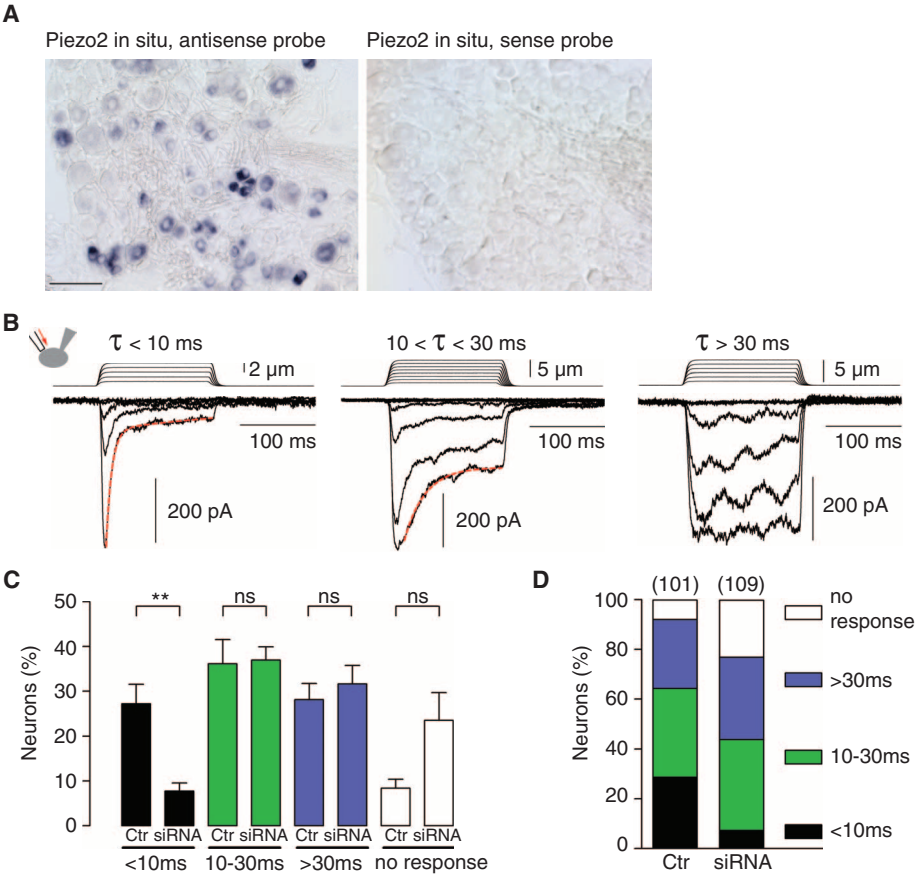

Fig. 6. Sensitivity of fast-inactivating MA currents in DRG neurons to depletion of Piezo2. (**A**) Representative images of colorimetric in situ hybridization for Piezo2 in DRG neurons by using (left) antisense and (right) sense probes. (**B**) Representative traces of three typical MA inward currents expressed in DRG neurons are characterized by distinct inactivation kinetics. Neurons were subjected to a series of mechanical steps in 1-µm increments at a holding potential of –80 mV. Current inactivation was fitted with (left) a bi-exponential equation, giving fast time-constant (τ) of 7.3 ms and slow time-constant > 100 ms, or (middle) a mono-exponential equation, giving a time constant of 27 ms. Some currents with τ > 30 ms are too slow to be efficiently fitted during the (right) 150-ms step stimulation. (**C** and **D**) Frequency histograms indicating the proportion of neurons transfected with scrambled siRNA (Ctr) or Piezo2 siRNA (siRNA) that respond to mechanical stimulation, with MA currents characterized by their inactivation kinetic. Bars represent the mean ± SEM of (B) the proportion of neurons from seven separate experiments (n = 12 to 19 neurons per condition and per experiment) or (C) the proportion from all neurons pooled from all seven experiments; the numbers above bars in (C) represent the number of neurons. $^{**}P < 0.01$; ns, not significantly different; unpaired t test.

proper expression or for modulating channel properties, similar to β subunits of voltage-gated channels (*32*) or SUR subunits of adenosine 5′-triphosphate–sensitive K+ channels (*33*). In this case, all the cell types used here would have to express an inactive conducting subunit of an MA channel that requires Piezos to function. Alternatively, Piezo proteins may define a distinct class of ion channels, akin to Orai1, which lacks sequence homology to other channels (*34*). Piezo1 is also found in the endoplasmic reticulum (*14*, *15*), so Piezos may act at both the plasma membrane and in intracellular compartments.

We described a role of Piezo2 in rapidly adapting MA currents in somatosensory neurons. Thus, Piezo2 has potential roles in touch and pain sensation (*35*, *36*). Piezo1 and Piezo2 are expressed in various tissues, and their homologs are present throughout animals, plants, and protozoa, raising the possibility that Piezo proteins have a broad role in mechanotransduction.

References and Notes

1. M. Chalfie, *Nat. Rev. Mol. Cell Biol.* **10**, 44 (2009).
2. O. P. Hamill, B. Martinac, *Physiol. Rev.* **81**, 685 (2001).
3. G. B. Monshausen, S. Gilroy, *Trends Cell Biol.* **19**, 228 (2009).
4. K. Iwatsuki, T. Hirano, *Comp. Biochem. Physiol. Physiol.* **110**, 167 (1995).
5. D. P. Corey, A. J. Hudspeth, *Biophys. J.* **26**, 499 (1979).
6. G. C. McCarter, D. B. Reichling, J. D. Levine, *Neurosci. Lett.* **273**, 179 (1999).
7. H. A. Praetorius, K. R. Spring, *J. Membr. Biol.* **184**, 71 (2001).
8. B. Coste, M. Crest, P. Delmas, *J. Gen. Physiol.* **129**, 57 (2007).
9. L. J. Drew, J. N. Wood, P. Cesare, *J. Neurosci.* **22**, RC228 (2002).
10. S. R. Besch, T. Suchyna, F. Sachs, *Pflugers Arch.* **445**, 161 (2002).
11. H. Cho *et al.*, *Eur. J. Neurosci.* **23**, 2543 (2006).
12. S. Earley, B. J. Waldron, J. E. Brayden, *Circ. Res.* **95**, 922 (2004).
13. R. Sharif-Naeini *et al.*, *Cell* **139**, 587 (2009).
14. K. Satoh *et al.*, *Brain Res.* **1108**, 19 (2006).
15. B. J. McHugh *et al.*, *J. Cell Sci.* **123**, 51 (2010).
16. R. O. Hynes, *Cell* **110**, 673 (2002).
17. G. Burnstock, *Mol. Pain* **5**, 69 (2009).
18. L. Rodat-Despoix, P. Delmas, *Pflugers Arch.* **458**, 179 (2009).
19. J. Hu, G. R. Lewin, *J. Physiol.* **577**, 815 (2006).
20. L. J. Drew *et al.*, *J. Physiol.* **556**, 691 (2004).
21. L. J. Drew *et al.*, *PLoS ONE* **2**, e515 (2007).
22. C. Wetzel *et al.*, *Nature* **445**, 206 (2007).
23. J. Hao *et al.*, in *Mechanosensitivity of the Nervous System*, I. K. e. A. Kamkin, Ed. (Springer Netherlands, 2008), vol. 2, pp. 51–67.
24. M. Schmidt, A. E. Dubin, M. J. Petrus, T. J. Earley, A. Patapoutian, *Neuron* **64**, 498 (2009).
25. Materials and methods are available as supporting material on *Science* Online.
26. M. E. Goldstein, S. B. House, H. Gainer, *J. Neurosci. Res.* **30**, 92 (1991).
27. S. N. Lawson, *Exp. Physiol.* **87**, 239 (2002).
28. S. N. Lawson, A. A. Harper, E. I. Harper, J. A. Garson, B. H. Anderton, *J. Comp. Neurol.* **228**, 263 (1984).
29. H. Sann, P. W. McCarthy, G. Jancsó, F. K. Pierau, *Cell Tissue Res.* **282**, 155 (1995).
30. M. Bandell *et al.*, *Neuron* **41**, 849 (2004).
31. S. E. Jordt *et al.*, *Nature* **427**, 260 (2004).
32. M. R. Hanlon, B. A. Wallace, *Biochemistry* **41**, 2886 (2002).
33. S. J. Tucker, F. M. Ashcroft, *Curr. Opin. Neurobiol.* **8**, 316 (1998).
34. M. Prakriya *et al.*, *Nature* **443**, 230 (2006).
35. A. I. Basbaum, D. M. Bautista, G. Scherrer, D. Julius, *Cell* **139**, 267 (2009).
36. G. R. Lewin, R. Moshourab, *J. Neurobiol.* **61**, 30 (2004).

37. The authors gratefully acknowledge H. Hu for help in cloning Piezo2, J. Walker for contributing to microarray experiments, S. Batalov for help in bioinformatics analysis, K. Spencer for help with imaging, and N. Hong and U. Müller for comments on the manuscript and helpful discussions. This work was supported by grants from NIH (DE016927 and NS046303) and the Novartis Research Foundation. B.C. is the recipient of an American Heart Association postdoctoral fellowship; M.S. is the recipient of a German Academic Exchange Service (DAAD, D/07/41089) fellowship. A provisional patent has been filed by TSRI and GNF that claims methods of screening for molecules that modulate Piezo-dependent ion channel activities. The Piezo1 and Piezo2 sequences used in the paper have been deposited in GenBank under accession numbers HQ215520 and HQ215521, respectively.

Supporting Online Material

www.sciencemag.org/cgi/content/full/science.1193270/DC1
Materials and Methods
Figs. S1 to S8
Tables S1 and S2
References

4 June 2010; accepted 20 August 2010
Published online 2 September 2010;
10.1126/science.1193270
Include this information when citing this paper.

REPORTS

Universal Dynamical Decoupling of a Single Solid-State Spin from a Spin Bath

G. de Lange,[1] Z. H. Wang,[2] D. Ristè,[1] V. V. Dobrovitski,[2] R. Hanson[1]*

Controlling the interaction of a single quantum system with its environment is a fundamental challenge in quantum science and technology. We strongly suppressed the coupling of a single spin in diamond with the surrounding spin bath by using double-axis dynamical decoupling. The coherence was preserved for arbitrary quantum states, as verified by quantum process tomography. The resulting coherence time enhancement followed a general scaling with the number of decoupling pulses. No limit was observed for the decoupling action up to 136 pulses, for which the coherence time was enhanced more than 25 times compared to that obtained with spin echo. These results uncover a new regime for experimental quantum science and allow us to overcome a major hurdle for implementing quantum information protocols.

In the past decade, manipulation and measurement of single quantum systems in the solid state have been achieved (*1*, *2*). This control has promising applications in quantum information processing (*3*, *4*), quantum communication (*5*), metrology (*6*), and ultrasensitive magnetometry (*7*, *8*). However, uncontrolled interactions with the surroundings inevitably lead to decoherence of the quantum states (*9*) and pose a major hurdle for realizing these technologies. Therefore, the key challenge in current experimental quantum science is to protect individual quantum states from decoherence by their solid-state environment.

If a quantum system can be controlled with high fidelity, dynamical decoupling can be exploited to efficiently mitigate the interactions with the environment (*10*–*12*). By reversing the evolution of the quantum system at specific times with control pulses, the effect of the environment accumulated before the pulse is canceled during the evolution after the pulse. When viewed at the end of the control cycle, the quantum system will appear as an isolated system that is decoupled from its environment. Thanks to recent progress in quantum control speed and precision (*13*, *14*), we can now unlock the full power of dynamical decoupling at the level of a single spin.

We focused on electron spins of single nitrogen-vacancy (NV) defect centers in diamond coupled to a spin bath (Fig. 1A). NV center spins can be optically imaged, initialized, and read out, as well as coherently controlled at room temperature (Fig. 1B). These favorable properties have been exploited to gain deeper insight into spin decoherence (*15*, *16*), as well as for demonstrating basic quantum information protocols at room temperature (*17*, *18*).

We used nanosecond microwave pulses to manipulate single NV spins. To raise the fidelity of our control to the required level for efficient decoupling, we fabricated on-chip coplanar waveguide (CPW) transmission lines using electron beam lithography (Fig. 1A). The high bandwidth of the CPW (*13*) combined with efficient suppression of reflections and fine-tuned pulse calibration (*14*) allows fast and precise manipulation of

[1]Kavli Institute of Nanoscience Delft, Delft University of Technology, Post Office Box 5046, 2600 GA Delft, Netherlands. [2]Ames Laboratory and Iowa State University, Ames, IA 50011, USA.

*To whom correspondence should be addressed. E-mail: r.hanson@tudelft.nl